ORIGINAL ARTICLE

WILEY

Three-dimensional non-isothermal numerical model for predicting semi-volatile organic compound transport process in a room

Fan Bai[1] [ID] | Hao Ding[1] | Yu-Tong Mu[2] | Yan-Jun Dai[1] | Yin-Ping Zhang[3] | Wen-Quan Tao[1] [ID]

[1]Key Laboratory of Thermo-Fluid Science & Engineering of MOE, Xi'an Jiaotong University, Xi'an, China

[2]School of Human Settlements and Civil Engineering, Xi'an Jiaotong University, Xi'an, China

[3]Institute of Built Environment, Tsinghua University, Beijing, China

Correspondence
Wen-Quan Tao, Key Laboratory of Thermo-Fluid Science & Engineering of MOE, Xi'an Jiaotong University, Xi'an, Shaanxi 710049, China.
Email: wqtao@mail.xjtu.edu.cn

Abstract

In this paper, a three-dimensional non-isothermal computational model for predicting indoor SVOC distribution is proposed, considering the effects of turbulence diffusion and suspended particles. The realizable k-ε model is introduced for turbulent flow simulation in a room. The Euler-Euler method is adopted to deal with the gas-particle two-phase flow coupled problem. Inertia slip velocity and irreversible first-order absorption boundary are employed for more accurate prediction of particle motion. The simulated curve of outlet gas-phase di-2-ethylhexyl phthalate (DEHP) concentration with emission time is verified by available experimental data. The emission process of DEHP in a 15 m^2 room in Beijing during 100 days with or without air cleaner is simulated by the developed model considering air leak through window and door gaps. It is found that if the air cleaner keeps on all the time during 100 days the gas-phase DEHP concentration in the room will tend to be uniform, while the emission process is far from equilibrium without an air cleaner even the emission lasts 100 days. Results also suggest that floor heating, decrease of particle concentration, weaken of heat transfer, enhancement of mass transfer, and air infiltration in window gap contribute to decrease DEHP concentration.

KEYWORDS
convective mass transfer, di-2-ethylhexyl phthalate, first-order absorption boundary, inertia slip velocity, numerical simulation model, semi-volatile organic compound

1 | INTRODUCTION

Nowadays, organic materials and their products are widely existing in a room, such as additives, polyvinylchloride (PVC) products, chemical commodities, etc. These materials can continuously release the alleged semi-volatile organic compounds (SVOCs), which are organic compounds that have a boiling point of 240–400°C.[1] It has been confirmed that SVOCs may cause various kinds of diseases,

for instance, allergy, endocrine imbalance, disorder of metabolism, etc.[2,3]

With the purpose of studying the transport and diffusion characteristics of SVOCs, their emission characteristics from indoor source materials must be revealed. SVOC emission process has been experimentally[4–9] and numerically[10–15] studied by a considering number of researchers. Their studies mainly focus on the SVOC concentration variation in a number of experimental chambers, such as Field and

Laboratory Emission Cell (FLEC)[16,17] etc., within which the studied source materials exist.

Hu and Chen established[11] and later improved[12,13] a mathematical model including laminar flow field, gas-phase DEHP concentration field and particle-phase DEHP concentration field. In their research, the SVOC concentration distributions in chambers are simulated. However, for the transport and diffusion of SVOCs in a real room, the above models should be extended in the following three aspects. (a) The present simulations are based on isothermal condition which is good enough to simulate the SVOC concentration evolution in a small test chamber. For a real room, the influence of temperature on SVOC emission characteristics has not been fully modeled. Previous experimental results have shown great impact of temperature on the emissions of SVOCs.[5,7–9] Wu et al.[18] exhibited that temperature in a room may differ 10 K, showing that temperature may be diverse in different positions of a room. Present isothermal model may cause an error due to a high response of temperature on the SVOC surface absorption characteristics.[5] (b) The concentrations of particle-phase SVOCs are affected by suspended particle concentration in the room.[10] In the numerical model, boundary conditions play an important role on the accuracy of the physical field prediction. However, the boundary conditions of suspended particle concentration equation assumed in the previous work do not match real-world conditions. Damkohler number (Da) is defined as the dimensionless absorption rate on the wall.[19] In the previous study of CFD simulation about FLEC, steel is used as the absorption surface, boundary condition of which is either assumed zero (full absorption boundary, $Da \to \infty$), or no flux boundary (full reflect boundary, $Da \to 0$). Whereas the actual wall of a room, Da value is finite.[19] (c) The importance of flow turbulence should be taken more into account. In FLEC, the flow is regular and laminar. However, in an actual room, the flow field is very complex and flow turbulence needs to be considered.[20,21] Furthermore, turbulent pulsating velocity will have an impact on the scalar transport[22] in a room. Therefore, in the simulation of species transport equation in a room, it would be more accurate considering turbulent pulsating effect.[23]

The objective of this paper is to improve numerical model through the above-mentioned three aspects: (a) to develop non-isothermal SVOC emission process prediction model and to show the superiority of non-isothermal model compared with the isothermal model in some circumstances, (b) to introduce an irreversible one-order absorption model near the wall for particle absorption and to show the more consistence of that with the experimental data compared with full absorption boundary and full reflect boundary, (c) to introduce turbulent pulsating effect and an inertia slip velocity into the governing equations referring to the parameters in the literature. The logic of this paper is organized as follows. In Section 2, a 3D numerical model for predicting indoor SVOC variation including turbulent flow, heat transfer (conduction, convection, and radiation), particle motion, gas-phase, and particle-phase DEHP distribution is established. In Section 3, the numerical model is verified by two experiments, deposition experiment of particles in a single room and

Practical Implications

Our study proposes a comprehensive three-dimensional non-isothermal SVOC emission and transport model. An irreversible first-order model is provided to simulate PM2.5 absorption boundary, the correction and necessity of this model are clarified. An actual bare room including PM2.5 air cleaner, window/door gaps, and floor heating is simulated. DEHP distribution characteristics with and without air cleaner are analyzed and compared in detail. These findings are useful for developing SVOC emission and transport numerical model, and also reveal the essential effects of convection and temperature non-uniformity on SVOC transport process in a room.

DEHP transport process experiment without suspended particles in FLEC. The emission processes of DEHP from PVC floor in a 15 m² bedroom in Beijing are simulated with PM2.5 air cleaner being on and off. Simulation results for 100 days in winter are presented and discussed in detail as well. Finally, Section 4 summarizes the findings and draws some important conclusions.

2 | NUMERICAL METHOD

There are two phases of SVOCs in indoor air: gas-phase and particle-phase. In this paper, Euler method is used to deal with this coupled gas-particle two-phase flow problem. The gas-phase SVOC concentration (c_{gp}, µg/m³) distribution is calculated by the continuum medium multi-component model. The particle concentration (c_p, µg/m³) and volume-average SVOC concentration attaching to suspended particles (c_{pp}, µg/m³) are simulated by convection-diffusion equations considering velocity slip between particle and gas.

2.1 | Gas-phase SVOC transport in the air

Flow field in a room is governed by Reynolds-time averaged continuity equation and momentum equation, as shown below,

$$\frac{\partial}{\partial x_i}(\rho_g u_i) = 0 \tag{1}$$

$$\frac{\partial(\rho_g u_j)}{\partial \tau} + \frac{\partial(\rho_g u_i u_j)}{\partial x_i} = -\frac{\partial p}{\partial x_j} + \frac{\partial}{\partial x_i}\left[(\mu + \mu_t)\frac{\partial u_j}{\partial x_i}\right] - \delta_{j3}\rho_g g \tag{2}$$

where x_i and x_j (m) are the direction vectors, u_i and u_j (m/s) are the time-averaged velocities, p (Pa) is time-averaged pressure, μ (Pa·s) and μ_t are molecular viscosity and turbulent viscosity, respectively, g (m/s²) is the gravity acceleration, ρ_g (kg/m³) is the density of the air and δ_{ij} (unit: 1)

is the Kronecker symbol, number "3" in which means the direction of gravity and $\delta_{33} = 1.0$.

In Equation (2), ρ_g varies with space. For considering the natural convection in a room, the Boussinesq approximation is applied,[24] and the density in the gravitational term in the momentum equation can be written as

$$\rho_g = \rho_{g0}\left[1 - \gamma(T - T_0)\right] \tag{3}$$

in which, T_0 (K) is reference temperature, ρ_{g0} is the density of the air at T_0, γ (K^{-1}) is the thermal expansion coefficient.

For the turbulence flow in a room, the realizable k-ε model is used which has been shown successfully in the study of Wang et al.[20,21] The governing equations of the turbulence fluctuation kinetic energy k (m^2/s^2) and its dissipation rate ε (m^2/s^3) are

$$\frac{\partial}{\partial \tau}(\rho_g k) + \frac{\partial}{\partial x_i}(\rho_g k u_i) = \frac{\partial}{\partial x_j}\left[\left(\mu + \frac{\mu_t}{Pr_k}\right)\frac{\partial k}{\partial x_j}\right] + G_k + G_b - \rho_g \varepsilon \tag{4}$$

$$\frac{\partial}{\partial \tau}(\rho_g \varepsilon) + \frac{\partial}{\partial x_i}(\rho_g \varepsilon u_i) = \frac{\partial}{\partial x_j}\left[\left(\mu + \frac{\mu_t}{Pr_\varepsilon}\right)\frac{\partial \varepsilon}{\partial x_j}\right] + C_{1\varepsilon}\rho S\varepsilon - C_{2\varepsilon}\rho\frac{\varepsilon^2}{k + \sqrt{\mu\varepsilon/\rho}} + C_{3\varepsilon}\frac{\varepsilon}{k}G_b \tag{5}$$

where $\quad C_{1\varepsilon} = max\left(0.43, \frac{Sk}{Sk+5\varepsilon}\right)$, $\quad S = \sqrt{2S_{i,j}S_{i,j}}$, $\quad S_{i,j} = \frac{1}{2}\left(\frac{\partial u_i}{\partial x_j} + \frac{\partial u_j}{\partial x_i}\right)$,

$C_{3\varepsilon} = \tanh\left|\frac{(\delta_{j3}u_j)}{\sqrt{(u_i u_i)}}\right|$

$C_{2\varepsilon}$ is constant, Pr_k and Pr_ε are the turbulent Prandtl number for k and ε, respectively, and G_k (kg/m/s^3) and G_b (kg/m/s^3) are turbulence kinetic energy generation due to the local mean velocity gradients and the buoyancy, respectively, which can be calculated by

$$G_k = \mu_t S^2, \quad G_b = \alpha_V g_i \frac{\mu_t}{Pr_T}\frac{\partial T}{\partial x_i} \tag{6}$$

in which, Pr_T is turbulent Prandtl number for temperature.

Turbulent viscosity μ_t can be obtained by

$$\mu_t = \rho_g C_\mu \frac{k^2}{\varepsilon} \tag{7}$$

The coefficient C_μ is calculated by

$$C_\mu = \frac{1}{A_0 + A_s\sqrt{S_{ij}S_{ij}}\frac{k}{\varepsilon}} \tag{8}$$

where

$$A_0 = 4.04, \quad A_s = \sqrt{6}\cos\phi, \quad \phi = \frac{1}{3}\cos^{-1}\left(\frac{\sqrt{6}S_{ij}S_{jk}S_{ki}}{\left(\sqrt{S_{ij}S_{ij}}\right)^3}\right) \tag{9}$$

For wall treatment of turbulence model, enhanced wall function treatment is adopted.[25] Parameters in the turbulent model $C_{2\varepsilon}$ in Equation (5), Pr_k in Equation (4), Pr_ε in Equation (5), Pr_T in Equation

(6) and Pr_s (wall Prandtl number in enhanced wall function treatment[25]) take values of 1.9,[26] 1.0,[22,26] 1.2,[22,26] 0.85[27,28] and 0.85,[28] respectively.

Based on the calculated fluid flow field, the time-averaged mass concentrations of gas-phase SVOCs can be obtained by a convection-diffusion equation[22]

$$\frac{\partial(c_{gp})}{\partial \tau} + \frac{\partial(u_i c_{gp})}{\partial x_i} = \frac{\partial}{\partial x_j}D_{gp,eff}\frac{\partial c_{gp}}{\partial x_j} - S_{c,g-p} \tag{10}$$

In the equation, the influence of turbulence is considered by an effective diffusion coefficient ($D_{gp,eff}$, m^2/s) instead of D_{gp} in the general convection-diffusion equation.[22]

$$D_{gp, eff} = D_{gp} + D_{gp,t} = D_{gp} + \frac{\mu_t}{Sc_{t,gp}\rho_g} \tag{11}$$

in which $Sc_{t,gp}$ is turbulent Schmidt number of DEHP. For high-content gas components in the flow (for instance, nitrogen and oxygen in the air), $Sc_{t,gp}$ is assumed as 0.7.[28] For trace suspended particles, $Sc_{t,gp}$ is assumed as 1.0.[23,29] SVOCs in indoor air are trace gas components in the flow. Therefore, $Sc_{t,gp}$ is assumed as 0.9.

It has been revealed by Lyman[5,30] that the effect of temperature on the diffusion coefficient of gas-phase SVOCs in the air can be expressed by

$$D_{gp} = D_{ref}\left(\frac{T}{T_{ref}}\right)^{1.75} \tag{12}$$

in which T_{ref} = 296 K, D_{ref} = 3.46 × 10^{-6} m^2/s.

$S_{c,g-p}$ in Equation (10) is the DEHP source term which shows how much gas-phase SVOCs transfers to particle phase, determined as follows:

$$S_{c, g-p} = h_m\left[N_p A_p c_{gp} - \frac{6c_{pp}}{K_p d_p}\right] \tag{13}$$

where c_{pp} is the particle-phase SVOC concentration. The derivation of Equation (13) is based on the literature of Hu et al.[11] with some modifications. The derivation details are shown in the Appendix S2.

In Equation (13), K_p (unit: 1) is the particle surface partition coefficient whose value will be discussed later, and h_m (m/s) is the mass transfer coefficient, calculated according to Cao's literature[31]

$$h_m = \frac{2D_{gp}}{d_p}\frac{1 + Kn}{1 + 0.377Kn + 1.333Kn\frac{(1 + Kn)}{\alpha}} \tag{14}$$

where α is the mass accommodation coefficient which takes 0.2,[31] Kn is Knudsen number calculated from[11]

$$Kn = \frac{2l_g}{d_p}, \quad l_g = \frac{3D_{gp}}{u_a}, \quad u_a = \sqrt{\frac{8RT}{\pi M}} \tag{15}$$

where R (8.314 J/mol/K) is the gas constant, l_g (m), u_a (m/s), M (0.391 kg/mol for DEHP) are the mean free paths of SVOCs, mean molecular speeds, molecular weights of SVOCs, respectively.

It should be noted that the emissions of SVOCs are subjected to external convection control and the concentration distributions of SVOCs within emission plate are nearly uniform.[17] The concentrations of the gas-phase SVOCs near the emission surface can be seen as constant[13] at a specific temperature. Thus in the present paper, the emission model is simplified as the following temperature-dependent Dirichlet boundary condition for the gas-phase SVOC transport equation.

$$c_{gp}\big|_s = \frac{c_s}{K_s} \quad (16)$$

where c_s (µg/m²) is the interior surface concentration of SVOCs which is assumed as constant,[13,17] K_s (m) is surface partition coefficient of the emission surface. The impact of temperature (or floor heating) can be reflected on its influence on the surface partition coefficient of emission surface.

The condition of the absorption surface boundary is shown by Equation (17).[11]

$$D_{gp,eff} \frac{\partial(c_{gp})}{\partial \mathbf{n}}\bigg|_s = K_s \frac{\partial(c_{gp})}{\partial \tau} \quad (17)$$

where K_s is the surface partition coefficient of the absorption surface.

Surface partition coefficients on surfaces (Equations 16 and 17) and suspended particles (Equation 13) are affected by temperature. It has been revealed by Zhang et al.[32] that the effect of temperature on surface partition coefficient can be expressed by

$$K_{s/p} = C_1 T^{1/2} \exp(C_2/T) \quad (18)$$

in which C_1, C_2 can be fitted by some experimental values.[4-6,11] For absorption surfaces, fitting results are shown in Table 1. For emission surface, substitute Equation (18) into Equation (16)

$$c_{gp}\big|_s = \frac{c_s}{C_1 \sqrt{T} \exp\left(\frac{C_2}{T}\right)} = \frac{c_{s,eff}}{\sqrt{T} \exp\left(\frac{C_2}{T}\right)} \quad (19)$$

$c_{s,eff}$ and C_2 take 8.29×10^{22} µg/m³·K⁰·⁵ and 1.48×10^4 K, respectively, which are calculated from the experimental equilibrium gas-phase DEHP concentrations in the reference temperatures (under 23°C, take 0.93 µg/m³; under 47°C, take 38.0 µg/m³[5]).

TABLE 1 Constants in surface partition coefficient

	Steel	Wall	Particle
C_1	1.61×10^{-18} m·K⁻⁰·⁵	5.33×10^{-24} m·K⁻⁰·⁵	4.90×10^{-16} K⁻⁰·⁵
C_2	13 178 K	17 336 K	17 336 K

Experimental research shows that humidity has little influence on surface partition coefficient of DEHP.[5,6] Hence, in this study, the influence of humidity on the emission process of DEHP is ignored. Whereas for other SVOCs, this influence may be considered.[33]

2.2 | Particle-phase SVOC transport in the air

It is of great importance to model particle motion accurately because particle-phase SVOCs are attached to the suspended particles in the air. Volume fraction of particles is a criterion to judge the coupling relation of particle and flow field. It is pointed out by Elghobashi,[34] and Alletto et al.[35] that influence of the particles on the continuous phase can be ignored for particle volume fraction smaller than about 10^{-6}. In this study, the volume fraction of particles is assumed to be lower than 2×10^{-10} (normal situation of a conventional living room), only the effect of flow field on particle motion need to be considered. The mainstream velocity of particle is assumed identical to the gas. Different from main flow field, two slip velocities of particles, settling slip velocity and inertia slip velocity, should be considered and introduced as follows.

The settling slip velocity of particle $u_{i,S}$ is caused by the different effects of gravity on air and particle, which can be calculated by Equation (20).[36]

$$u_{i,S} = \frac{\rho_p d_p^2 g_i}{18\mu} \quad (20)$$

Noting that Equation (20) is only applied for the case when $d_p > 1$ µm, $Re_p < 1$ (defined by particle diameter, slip velocity and gas viscosity) and ρ_p (assumed to be 1670 kg/m³[37]) $\gg \rho_g$. Particles like PM2.5 or PM10 satisfy these conditions.

According to the hypothesis, a single particle remains relatively static in the reference system (mainstream of airflow) at a constant velocity. When the airflow accelerates or turns around, an inertia acceleration $a_{i,I}$ (m/s²) needs to be introduced, as shown in Figure 1. This inertia acceleration can be obtained by the minus of material derivative of velocity
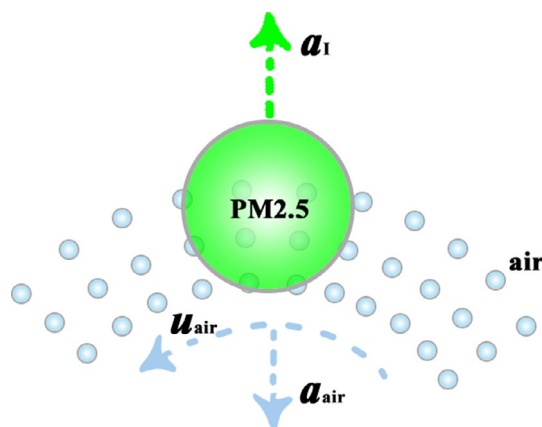

FIGURE 1 Inertia acceleration of suspended particle

$$a_{i,\mathrm{I}} = -\left(\frac{\partial u_i}{\partial \tau} + u_j \frac{\partial u_i}{\partial x_j}\right) \tag{21}$$

The inertia slip velocity $u_{i,\mathrm{I}}$ caused by the inertia force of particle can be calculated from[36]

$$u_{i,\mathrm{I}} = \frac{\rho_p d_p^2 a_{i,\mathrm{I}}}{18\mu} \tag{22}$$

Based on the above discussion, conservation of particle concentration can be obtained by

$$\frac{\partial(c_p)}{\partial \tau} + \frac{\partial\left[(u_i + u_{i,\mathrm{S}} + u_{i,\mathrm{I}})c_p\right]}{\partial x_i} = \frac{\partial}{\partial x_j}\left(D_{p,\mathrm{eff}}\frac{c_p}{\partial x_j}\right) \tag{23}$$

where $D_{p,\mathrm{eff}}$ (m^2/s) is the effective diffusion coefficient of particles

$$D_{p,\mathrm{eff}} = D_{p,b} + \frac{\mu_t}{Sc_{t,p}\rho_g} \tag{24}$$

$Sc_{t,p}$ is turbulent Schmidt number of the suspended particles which is assumed as 1.0.[23,29] $D_{p,b}$ is the diffusivity caused by Brownian movement,[38]

$$D_{p,b} = \frac{k_B T C_C}{3\pi\mu d_p} \tag{25}$$

where k_B (1.38×10^{-23} J/K) is the Boltzmann constant, C_C is Cunningham constant[36] which can be calculated from

$$C_C = 1 + \frac{\lambda_g}{d_p}\left[2.514 + 0.8\exp\left(-0.55\frac{d_p}{\lambda_g}\right)\right] \tag{26}$$

where λ_g (μm) is the mean free length of air molecules (0.066 μm at 293 K, 101 kPa).

Inlet boundary condition of c_p at window gap is assumed to be of the first type whose value takes the environmental particle concentration, as is shown in Table 1 of the Appendix S1. Boundary condition of particle concentration on the wall is assumed as absorption boundary condition,

$$-D_{p,\mathrm{eff}}\frac{\partial c_p}{\partial \mathbf{n}}\bigg|_s = \kappa_s c_p \tag{27}$$

where κ_s (m/s) is absorption rate of boundary, and $\mathbf{n}$ is the exterior normal-vector of the wall. The value of κ_s is difficult to measure and different under each individual surface condition. In this study, κ_s is approximately selected as an average value of a room, which is obtained by the overall loss rate β (s^{-1}) in the well-mixed mass-balance model[39] as follows.

First, for a well-mixed room we may assume:

$$\frac{dc_{p,a}}{d\tau} = -\beta c_{p,a} \tag{28}$$

where $c_{p,a}$ is the average particle concentration in the room. The lost particles are assumed to be absorbed by the room walls. Based on mass conservation law, we have

$$-\iiint_V \frac{\partial c_p}{\partial \tau}\,\mathrm{d}V = \iint_A -D_{p,\mathrm{eff}}\frac{\partial c_p}{\partial \mathbf{n}}\,\mathrm{d}A \tag{29}$$

Overall loss rates are experimentally studied for different particle diameters by Thatcher et al.[39] In their research, a well-mixed room, whose concentration of particles is nearly uniform, is studied. Assuming $c_{p,a} = c_p$, comparing Equations (27), (28) and (29), we have

$$\kappa_s = \frac{V_{\mathrm{room}}}{A_{\mathrm{room}}}\beta \tag{30}$$

In an actual room, the velocity is not high enough to guarantee the well-mixed character of suspended particles, thus local concentration of particles near the surface is used to calculate the absorption in Equation (27).

Particle-phase SVOCs are attached to the suspended particle. Based on the above equations about suspended particle (Equations 23–30), volume-average concentration of SVOCs attaching to suspended particles (particle-phase SVOCs) c_{pp} can be calculated by the following governing equation and boundary conditions:

$$\frac{\partial(c_{pp})}{\partial \tau} + \frac{\partial\left[(u_i + u_{i,\mathrm{S}} + u_{i,\mathrm{I}})c_{pp}\right]}{\partial x_i} = \frac{\partial}{\partial x_j}\left(D_{p,\mathrm{eff}}\frac{c_{pp}}{\partial x_j}\right) + S_{c,g\text{-}p} \tag{31}$$

$$-D_{p,\mathrm{eff}}\frac{\partial c_{pp}}{\partial \mathbf{n}}\bigg|_s = \kappa_s c_{pp} \tag{32}$$

$$c_{pp}\big|_{\mathrm{inlet}} = 0 \tag{33}$$

In Equations (13, 14, 15, 20, 22, 25, 26), diameter of the suspended particles (d_p) is included and assumed as 1.473 μm. Hinds[36] pointed out that the diameter of suspended particles in the air follows lognormal distribution, as shown in Equation (34).

$$f(d_p) = \begin{cases} \dfrac{1}{\sqrt{2\pi}\sigma d_p}\exp\left[-\dfrac{(\ln d_p - \mu)^2}{2\sigma^2}\right] & d_p > 0 \\ 0, & d_p \le 0 \end{cases} \tag{34}$$

in which μ is the average of the logarithms of the diameters, σ is the standard deviation of the logarithms of the diameters. They can be fitted from the experimental result.[40] Fitting result is μ = 2.1927 μm, σ = 1.2555 μm, and are shown in Figure 2. The average diameter lower than 2.5 μm can be calculated as Equation (35).

$$\stackrel{!!}{\mu} = \frac{\int_0^{2.5}\frac{1}{\sqrt{2\pi}\sigma}\exp\left[-\frac{(\ln d_p - \mu)^2}{2\sigma^2}\right]\mathrm{d}d_p}{\int_0^{2.5}\frac{1}{\sqrt{2\pi}\sigma d_p}\exp\left[-\frac{(\ln d_p - \mu)^2}{2\sigma^2}\right]\mathrm{d}d_p} = 1.473\ \mu\mathrm{m} \tag{35}$$
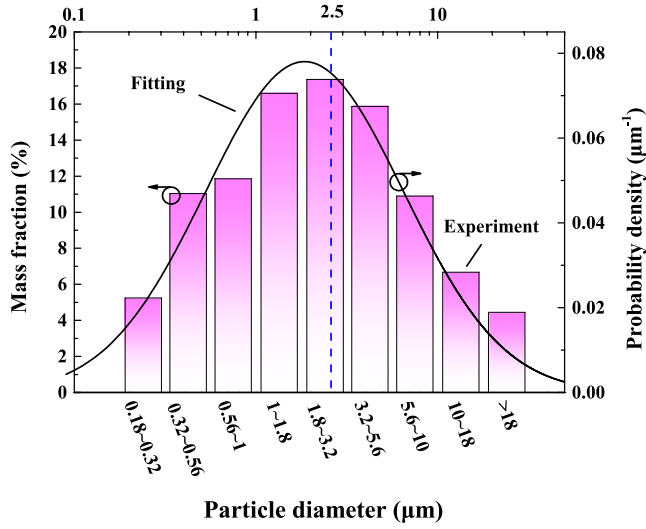
2.3 | Non-isothermal model

Temperature distribution follows energy equation and radiation heat transfer equation

$$\frac{\partial(\rho_g T)}{\partial \tau} + u_i \frac{\partial(\rho_g T)}{\partial x_i} = \frac{\partial}{\partial x_j}\left[\left(\frac{\lambda}{c_p} + \frac{\mu_t}{Pr_T}\right)\frac{\partial T}{\partial x_j}\right] \quad (36)$$

in which λ (W/m/K) is thermal conductivity and c_p (J/kg/K) is specific heat capacity. Temperatures of both the air and the solid regions (wall, door, window) are considered. Window gap inlet temperature is identical to the outdoor value, as is shown in Table 1 of the Appendix S1. Boundary condition of the room exterior wall and that of the indoor underground are considered as the convective boundary conditions

$$-\lambda \frac{\partial T}{\partial \mathbf{n}} = h(T_s - T_\infty) \quad (37)$$

where T_∞ is the average temperature of the heat transfer fluid (outer air or water in floor heating system). h (W/m²/K) is convective heat transfer coefficient. Since the temperatures of the room inner surfaces are to be determined during the simulation, and temperatures of different walls may be different, the radiation heat transfer between different walls should be taken into account.

The surface-to-surface radiation model[41] is applied for the radiation heat transfer among walls. Heat flux conservation equation of each surface element can be calculated by

$$q_i = e_i \sigma T_i^4 + (1 - e_i)\varphi_{i,j}q_j \quad (38)$$

where double subscript (j) implies summation over the room enclosure surfaces, q_i (W/m²) is the net efferent heat flux (radiosity), σ is Planck's

constant (5.67 × 10⁻⁸ W/m²/K⁴), e is emissivity of the wall which is assumed as 0.9,[42] and $\varphi_{i,j}$ is the angle factor between surface j and surface i which can be calculated by

$$\varphi_{i,j} = \frac{1}{A_i}\iint\limits_{A_i A_j} \frac{\cos\theta_i \cos\theta_j}{\pi r^2}\delta_{ij}dA_i dA_j \quad (39)$$

in which r (m) is the distance of the two surfaces, θ_i is the included angle between distance vector and surface normal direction of the infinitesimal surface. q_i can be obtained by the simultaneous solutions of Equation (38) in all surface elements. The flux of radiation heat transfer can be calculated by

$$q_{\text{rad},i} = \frac{e_i \sigma T_i^4 - q_i}{\frac{1 - e_i}{e_i}} \quad (40)$$

Equation (40) is treated as source term coupled of Equation (36) for the ground, ceiling, and the indoor air side of the walls.

2.4 | Numerical procedure

The above equations are solved by finite volume method in 64-core parallel ANSYS FLUENT 17.2 with user-defined function (UDF). Implicit method is used for transient simulation. Second-order upwind difference is applied for the discretizations of the convection terms in all of the equations. The flow field should be in steady-state at the initial time. The usual initialization method assumes the initial fields to be zero. This method failed to accurately predict the turbulence viscosity with an error of 2–4 order of magnitude. Turbulent viscosity is a critical factor in turbulent thermal conductivity and the turbulent diffusion coefficients of particle, gas-phase DEHP, particle-phase DEHP concentrations. Hence, the steady-state fluid and temperature fields are simulated at first and the results are used as the initial fields. The convergence criteria of the initial steady-state fields include both residuals <10⁻⁴ and relative change rate of average velocity and the turbulent viscosity lower than 0.1% within 2000 iteration steps.

3 | RESULTS AND DISCUSSION

3.1 | Validations of the present model

The above established non-isothermal model for predicting the transport process of indoor SVOCs is quite comprehensive. Apart from non-isothermal turbulent flow of air (governing Equations 1, 2, 4, 5, 36, and 38), it also includes the following three models: (1) The transport model of gas-phase SVOC concentration, Equation (10); (2) The transport model of particles, Equation (23), and (3) The transport model of particle-phase SVOCs, Equations (31–33). To the authors' knowledge, it is very difficult to find some experimental data that can verify all the above prediction models simultaneously.

Fortunately, we found two experimental studies which can provide some data for partial validation of our models.

3.1.1 | Deposition process of particle in a single room

Particle deposition plays an important role in the study of indoor SVOC transport characteristics. Special measurements were conducted in an isolated room[39] to study the particle deposition rate under different furnishing and indoor airflow conditions. The isolated room ($2.2 \times 2.7 \times 2.4$ m^3) is a closed room within which there are four electric fans and a particle generator generating particles in certain range of diameter, as shown in Figure 3A. The room is well-sealed, isolated from any external disturbances. The four fans are helped to create the well-mixed condition effectively. Typical measured results for particles with diameter from 1.7 to 2.1 μm in the room without furniture are shown in Figure 3. In the figure, the particle concentration value for the first 30 min represents the baseline of the particle concentration in the room. After 30 min, particles are emitted from the generator and particle concentration rises rapidly (about 3 min) to 61.5 cm^{-3}. In the simulation, the sorption rate of surface, κ_s, takes 9.88×10^{-5} m/s. Due to the mixing effect by the fans, the concentration decay rate becomes stable after three minutes of particle generation, and the linear part of the curve can be used to calculate the particle deposition rate.

This testing process is simulated by our models. Three grid and time step systems are examined, (a) grid number of 1.9026×10^6 and time step of 300 s, (b) grid number of 0.657×10^6 and time step of 300 s, (c) grid number of 1.9026×10^6 and time step of 1 s. Two additional cases with zero value particle boundary (full absorption boundary, Case (d)) and no flux particle boundary (full reflect boundary, Case (e)) are simulated under the same grid and time step system with Case (a). The simulated concentration variation with time is shown in Figures 3B and 3C . From Figure 3B, it can be seen that the results of the three grid-time step systems are almost the same and consistent with the test data very well. The result of system (b) can be regarded as the grid-independent and time-step-independent solution and the average relative deviation between systems (b) and

(c) is 0.72%. The average relative deviation between system (b) and the experiment result is 5.46%. From Figure 3C, we can see that the result with either zero value (full absorption) boundary or zero flux (full reflect) boundary shows a larger deviation compared with the experiment result, which indicates the necessity of first-order absorption boundary.

3.1.2 | DEHP transport process without particle in FLEC

A numerical FLEC model with the same size of an experimental model in Zhang's research[5,43] is built. As is shown in Figure 4A, DEHP emission surface (PVC) is put on the bottom of the test space. Steel absorption surface is set on the top of the model. Clean air flows into the chamber around the model. Dirty air with DEHP flows out of the chamber at the top outlet of the center. Airflow rate is 450 mL/min. Flow is assumed as laminar. Emission surface is assumed as a fixed concentration boundary while the absorption surface is assumed as a fixed flux boundary, numerically treated by Equations (16) and (17). c_{gp} at the emission surface is set as 38 μg/m^3. K_s of the absorption surface is 100. The grid independence assessment has been implemented, and the final grid number is 81 760. Time step is set as 0.1 s in the first 10 s, 1 s within 10 s ~ 1 min, 1 min within 1 min ~1 h, 15 min within 1 h ~1 day, and 30 min after 1 day.

The variation of the outlet DEHP concentration normalized by the bottom surface concentration versus time is shown in Figure 4B. We can see that the simulation results are consistent well with the experiment data.[5] The relative DEHP concentration increases rapidly to 0.4 at the very beginning time (first several seconds). The results of Hu et al.[11] and Xu et al.[44] reached the similar conclusion.

3.2 | Conditions of simulated room and grid system

The developed numerical models are now used to study the transient transport characteristics of DEHP for a 15 m^2 bedroom (see Figure 5) in Beijing in winter time. In this subsection, the simulation conditions and grid system will be presented and the simulation
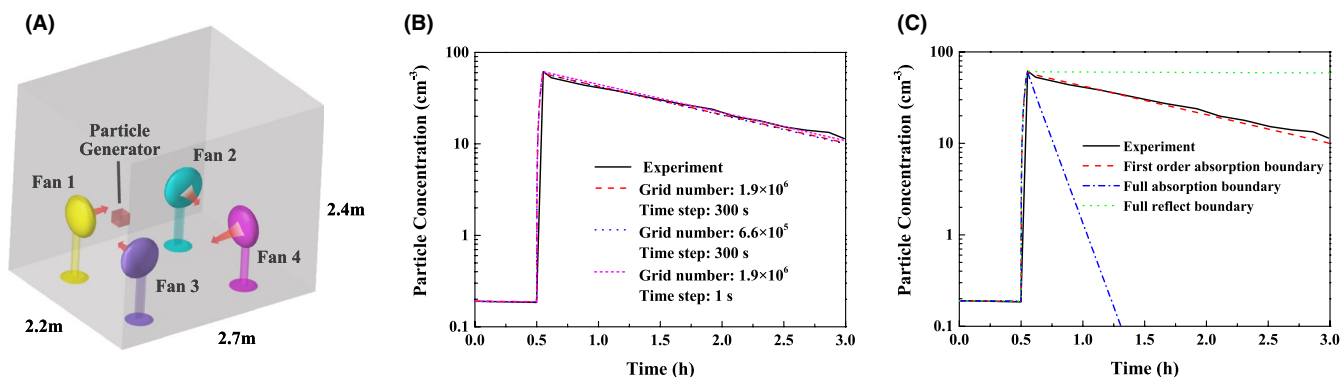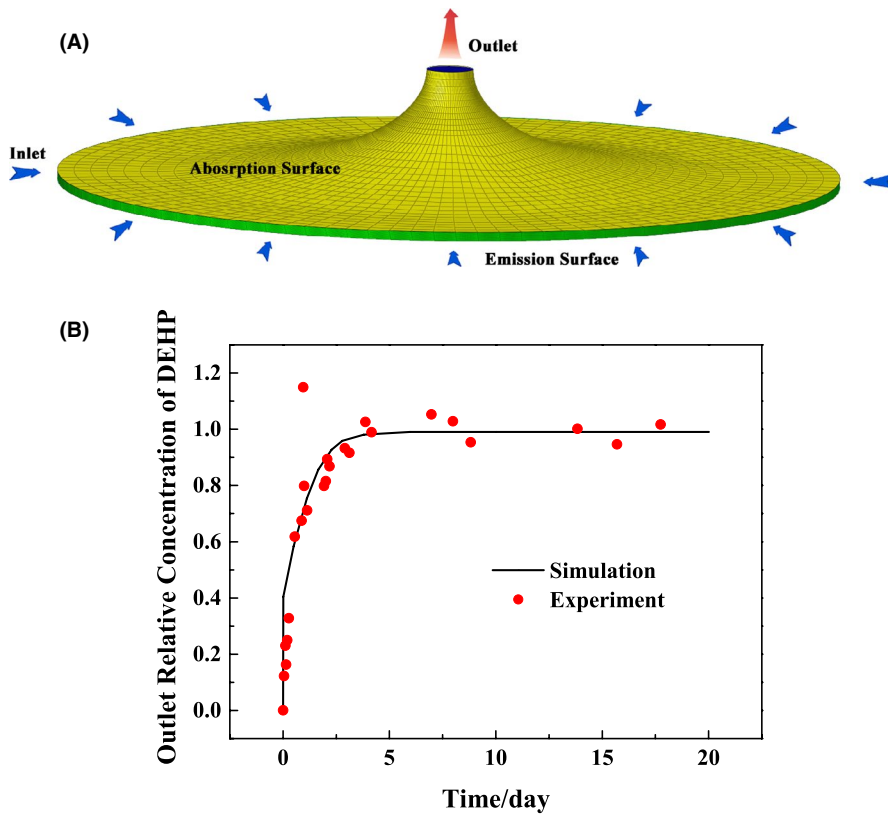

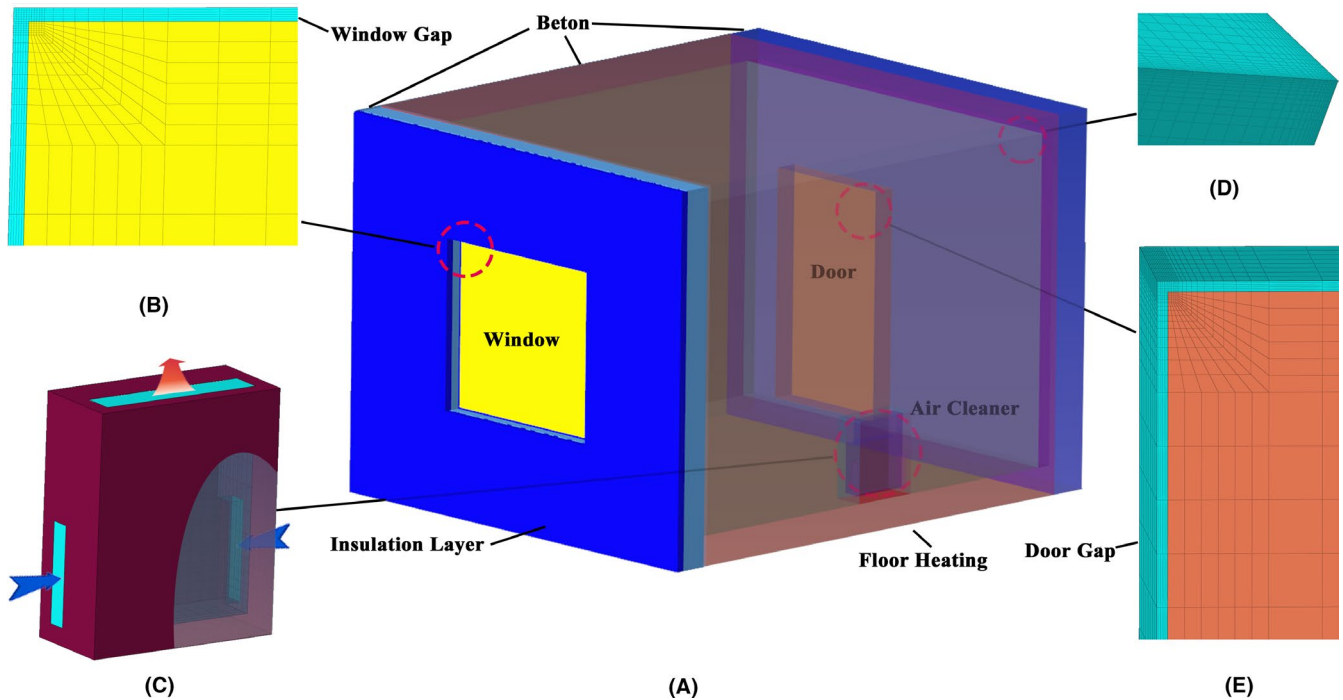**FIGURE 3** Particle deposition process

FIGURE 5 Computational domain of Beijing 15 m² bedroom

results of the transport characteristics in the room will be provided and discussed in Section 3.3.

The floor area of the room is 4.2 m × 3.6 m and the ceiling height is 2.9 m (volume = 43.8 m³). Outside wall (3.6 m × 2.9 m, facing toward south) is double-layer structure. Polystyrene heat preservation board (thickness: 0.07 m) is set as the outer layer for insulation. Beton is adopted as the inner layer (thickness: 0.25 m). Ceiling and other inner walls in the room are one-layer structure with beton (thickness: 0.2 m). 1.7 m × 1.5 m window with two-layer insulating glass is put in the center of the outside wall. Total thickness and center air

TABLE 2 Thermophysical properties of material in a room

	Inner beton	Outer beton	Steel	Window	Door	Polystyrene
ρ (kg/m³)	1000	1800	8030	2800	540	1050
c_p (J/kg/K)	1500	1278	502.48	705.36	2394	45.71
λ (W/m/K)	1	1.75	16.27	3.1	0.15	0.046

layer thickness of the window are 0.021 and 0.009 m, respectively. 1.2 m × 2.0 m wood door, 0.26 m distance from the west wall, is set in the north wall. Outside air flows into the room through the window gaps (16 mm) and out of the room through the door gaps (6 mm), gas-phase and particle-phase DEHP concentrations of which are assumed to be zero. Air change rate through the window gaps and door gaps is 0.2 h⁻¹, meaning that 20% of the air in the room is exchanged per hour. A PM2.5 air cleaner (length × width × height = 0.6 m × 0.2 m × 0.7 m) is set against east wall and 1.62 m distance from north wall for PM2.5 purification. Clean air delivery rate (CADR) of air cleaner is 168 m³/h. Floor heating system is established underground. Water temperature in the floor heating system is set as 40°C. For heating water and outdoor air, h is assumed as 3056 W/(m²·K) and 23 W/(m²·K)[42], respectively. Thermophysical properties of the materials are shown in Table 2. Local temperature is applied for all of the temperature-dependent parameters, such as D_{gp} in Equation (11), h_m in Equation (13), K_s in Equation (16), etc. The absorption rate of the surface, κ_s, takes 4.40×10^{-5} and 4.67×10^{-5} m/s when air cleaner "on" and "off", respectively (calculated from Figure 5 in Thatcher's literature[39] according to Equation 30).

Assumptions of the simulating room are listed as follows. (1) The room is assumed as a bare room with an air cleaner. Furnishings are not considered. (2) The influence of human movement on the indoor flow field is ignored. The flow field in the room is only caused by air cleaner and the ventilation leakage through window and door gaps. Air flows into the air cleaner through two opposite surfaces and out of that through the top surface, shown in Figure 5C. (3) Thermal boundary conditions of the exterior sides of the ceiling and walls (except outside wall) are assumed to be adiabatic boundaries due to the symmetry with other rooms. (4) Solar radiation on the outside wall is assumed as a surface heat source. (5) The PM2.5 air cleaner has a complete purification effect on PM2.5 and particle-phase DEHP but has no purification effect on gas-phase DEHP. (6) PVC floor is the only DEHP emission surface. Ceiling and walls are absorption surfaces, and initial room DEHP concentrations are 0. Related parameters of K_{surf} are shown in Table 1. (7) It's assumed that the environmental air has no DEHP in either gas-phase or particle-phase.

The actual meteorological data (temperature, solar radiation, and PM2.5 concentration, shown in Table 1 of the Appendix S1) are used as the outside environmental conditions for the boundary condition of outside wall and window gap. 90% and 38% (solar heat gain coefficient) of solar radiation heat enter into the room through the outside wall and window. Two cases (air cleaner state: on/off, called "on" case and "off" case, respectively, referring particularly to air cleaner state hereafter this paper) are simulated. In January 1st, new polyvinylchloride (PVC) flooring have just installed which will emit DEHP.

TABLE 3 Personal active time in the room

	Time segment when person is at home
Working day	0:00~7:00, 19:00~24:00
Weekend	0:00~8:00, 12:00~14:00, 21:00~24:00

In "on" case, when people stay in the room, the heating system will open otherwise it will turn off. Personal activity time in the room is shown in Table 3. In "off" case, floor heating is open all the time due to a low convection heat transfer. In both "on" case and "off" case, floor heating stops on March 15th. A period of 100 days is simulated.

Patched two-block multiple structural grid system is generated for simulation. The procedures are as follows. (1) First, as shown in Figure 5B, surface grids are generated on the corner of the window gap and door gap. Then the same surface grids are copied onto the corner of the window and door. (2) Then the two blocks of dense surface grids are projected to sparse grid on the windows and door surfaces, as is shown in Figures 5B,E. (3) Later, the surface grids on outside (south) wall and north wall are projected based on the edge of the window gap and door gap. (4) Finally, the two blocks of surface grids are projected to 3D grids along the 4.2 m edge. An interface is formed between the two blocks. Grid size variations near all the walls follow an exponential law, shown in Figure 5D. Total cell number is 2.91×10^6. Volumes of each grid cell is smaller than that in isolated room deposition test Case (b), where the mesh independent characteristics of this grid system are clearly demonstrated.

3.3 | Transport of SVOCs in the room with or without air cleaner

From numerical results the average values of temperature, PM2.5 concentration, gas-phase DEHP concentration, and particle-phase DEHP concentration at five horizontal planes, that are, floor plane, $z = 0.5$ m plane (nose height of a lying person), $z = 1.0$ m plane (nose height of a sitting person), $z = 1.55$ m plane (nose height of a standing person) and ceiling plane ($z = 2.9$ m) of the room, are presented in Figures 6 and 7 for "on" case and "off" case, respectively. In the figures, curves represent the values of concentration or temperature, and their locations are indicated by tached z-coordinate values.

Overall, in "on" case, as shown in Figure 6, the DEHP gas-phase concentration near the emission surface fluctuates rapidly in a narrow range. Temperature in the room is nearly uniform while that of the floor is a little higher due to an intense convection heat
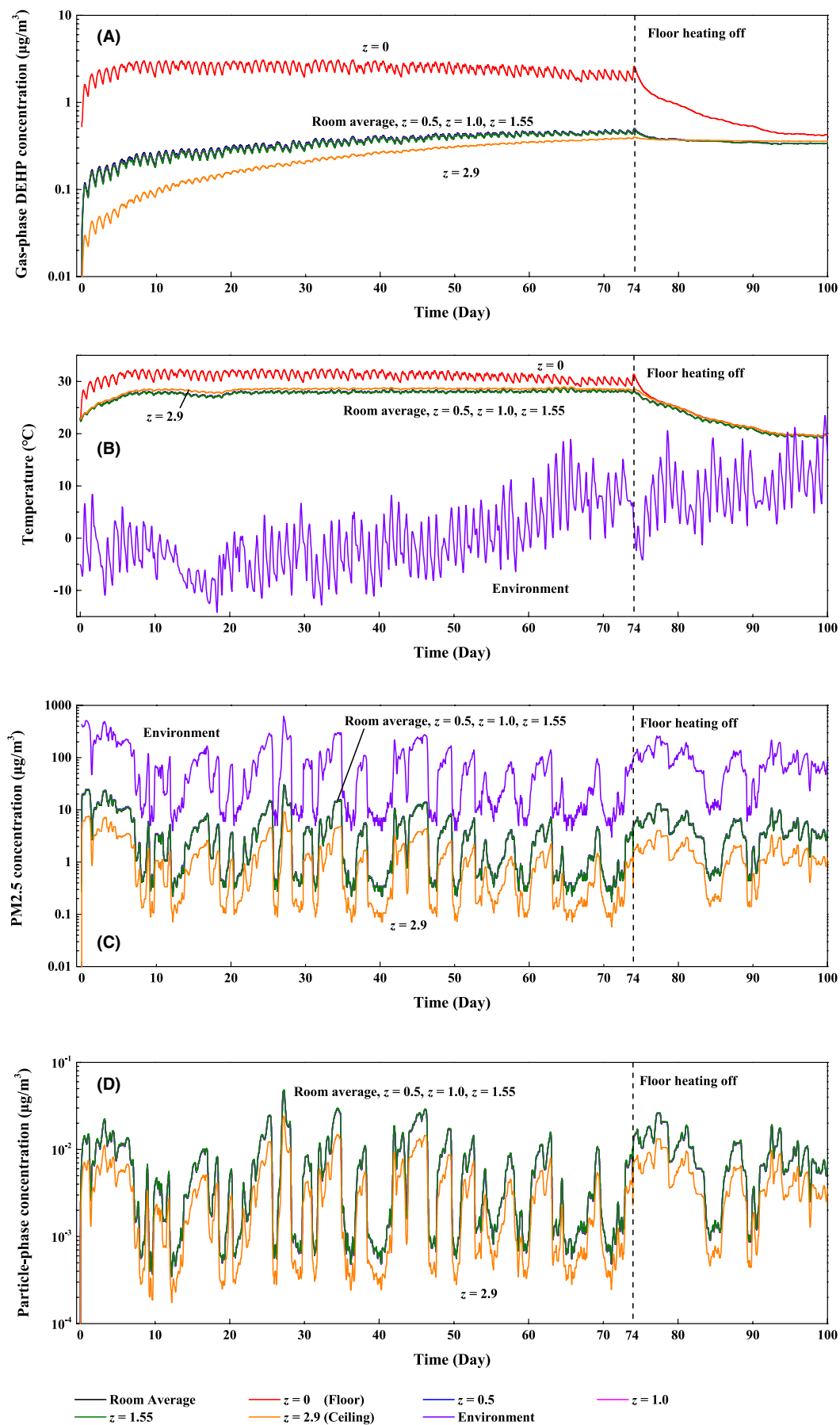
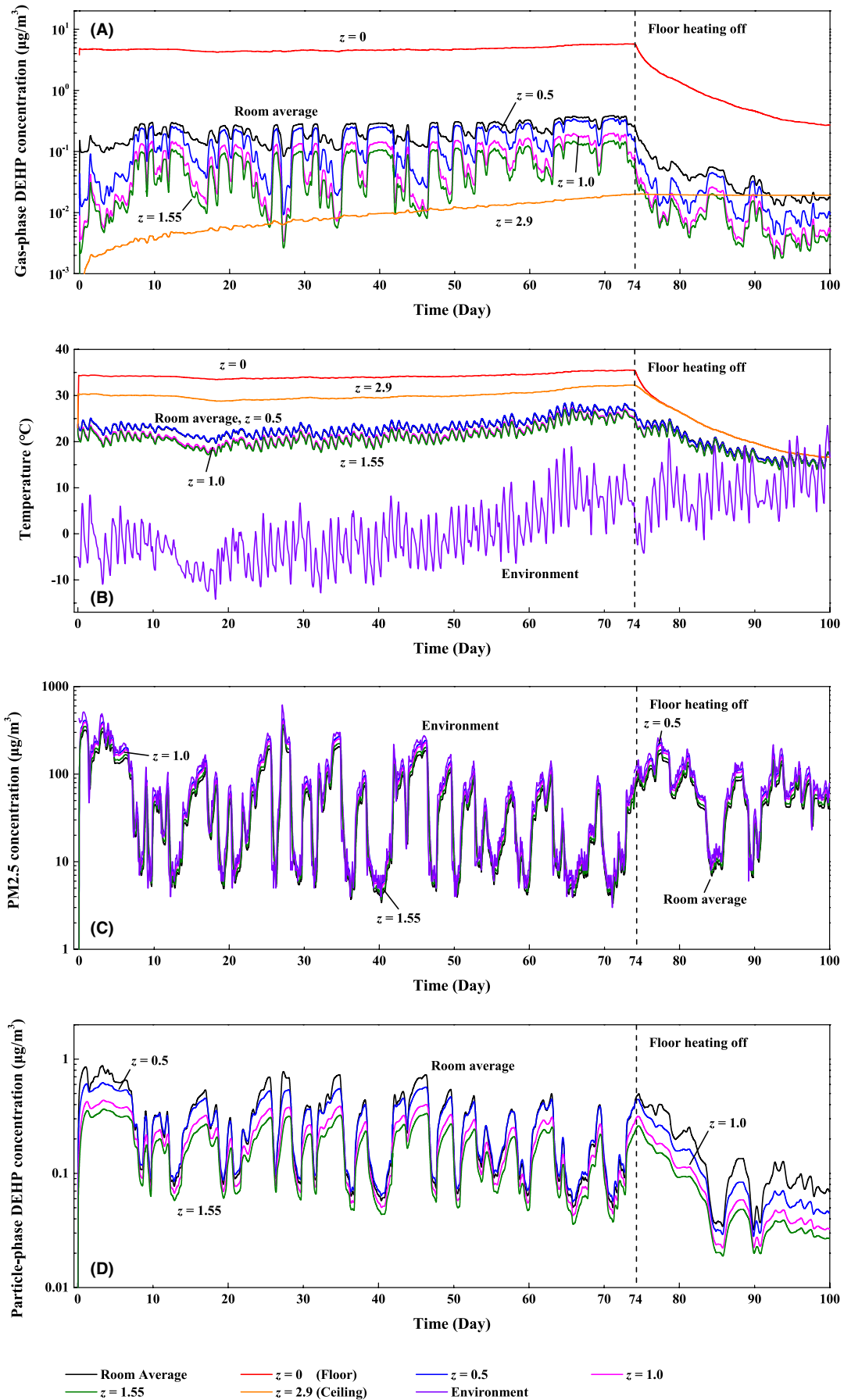**FIGURE 6** Simulation results of four parameters for air cleaner "on" case

FIGURE 7 Simulation results of four parameters for air cleaner "off" case

transfer. It should be noted that at the final state of DEHP emission process, DEHP concentration in the room will be equal to the concentration near the emission surface. This state is alleged as equilibrium state and the average DEHP concentration normalized by the DEHP concentration near the emission surface is equal to 1. In general, the room average value of DEHP concentration is an order of magnitude lower than that near the floor. Gas-phase DEHP concentrations near ceiling and floor (emission surface) are 0.396 and 2.498 $\mu g/m^3$, respectively, at the end of the 74th day, meaning that the emission DEHP is far from equilibrium state. After 74th day, the closing of heating leads to a sharp decrease of temperature in the floor, so does c_{gp} near the emission surface. Finally, gas-phase DEHP concentration in the room tends to be uniform. Floor heating and convection mass transfer jointly promote the emission process. Due to the deposition and the purification of PM2.5 by air cleaner, volume-average PM2.5 concentration is lower than 30 $\mu g/m^3$ in most of the time while particle-phase DEHP concentration is in the magnitude of 10^{-4} to 5×10^{-2} $\mu g/m^3$, which also contributes to the decrease of gas-phase DEHP concentration in the room due to the absorption of DEHP into PM2.5 and finally removed by the air cleaner.

In "off" case, as shown in Figure 7, floor temperature is the highest. Wall temperatures are medium due to the radiation effect and high heat conductivity of concrete wall. Air temperature is the lowest. A higher temperature near the emission surface leads to a higher DEHP concentration near the emission surface. Gas-phase DEHP concentrations near ceiling and floor are 0.020 and 5.707 $\mu g/m^3$, respectively, at the end of the 74th day, meaning that the emission process of DEHP is far from equilibrium state. Average PM2.5 concentration in the room is much higher than that in "on" case. Quantities of gas-phase DEHP attaches to the suspended particles, leading to the particle-phase DEHP concentration is 1–2 orders of magnitude higher than that in "on" case, which will finally settle on the floor or absorb onto the wall. After 74th day, with the turning off of floor heating, DEHP concentration near the floor is also decrease.

Finally, gas-phase DEHP concentrations near ceiling and floor are 0.019 and 0.271 $\mu g/m^3$, respectively, far from reaching equilibrium status.

Figures 8A and B show air path lines in "on" case and "off" case, respectively. In "on" case, the velocity caused by air infiltration is significantly lower than air cleaner outlet velocity. Airflow in the room is mainly driven by air cleaner, leading to violent convection heat and mass transfer. Therefore, room average, $z = 0.5$, $z = 1.0$ and $z = 1.55$ values are nearly in coincidence in "on" case (Figure 6). Several complex vortexes and violent convection are formed. However, in "off" case, airflow in the room is mainly driven by air infiltration through window gap and door gap. A few vortexes are formed at the corners near window gap.

There are three heat transfer modes in the room, heat conduction of concrete and heat preservation board, convection (natural convection and forced convection) of the air, and radiation among inner walls. Figures 9A and B give the temperature distributions on the y-direction middle cross-section after 1 day in "on" case and "off" case, respectively. As shown, in "on" case, the violent forced convection is dominant, leading to a relatively uniform temperature field. Therefore in "on" case, room average temperature rapidly rises (Figure 6B). In contrast, in "off" case, forced convection effect is not intensive enough to make the temperature field uniform. Floor heating process is slow and radiation heat transfer is dominant. Temperature near the ceiling is relatively high radiated from the heating floor. Room average temperature is largely determined by environmental temperature (Figure 7B) due to the air infiltration through window gap. Because of the slow convection, heat in the walls are difficult to release, leading to an extremely high wall temperature, especially on the floor (34°C approximately), as shown in Figure 9B. In addition, at the vertex zones on the upper and lower side of the window, air temperatures are higher due to a relative strong convection heat transfer. Furthermore, in "off" case, because of a higher floor temperature, the surface partition coefficient of the floor is lower compared with "on" case. According to Equation (16),
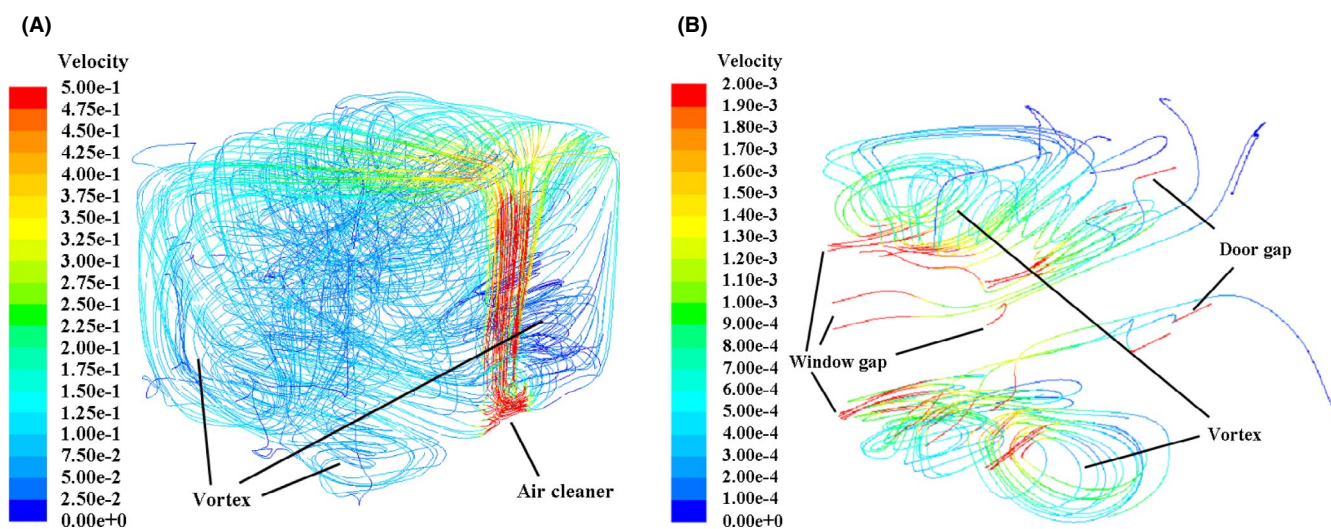

(A)

(B)

FIGURE 8 Path lines and velocity distribution clouds (m/s) after 1 day
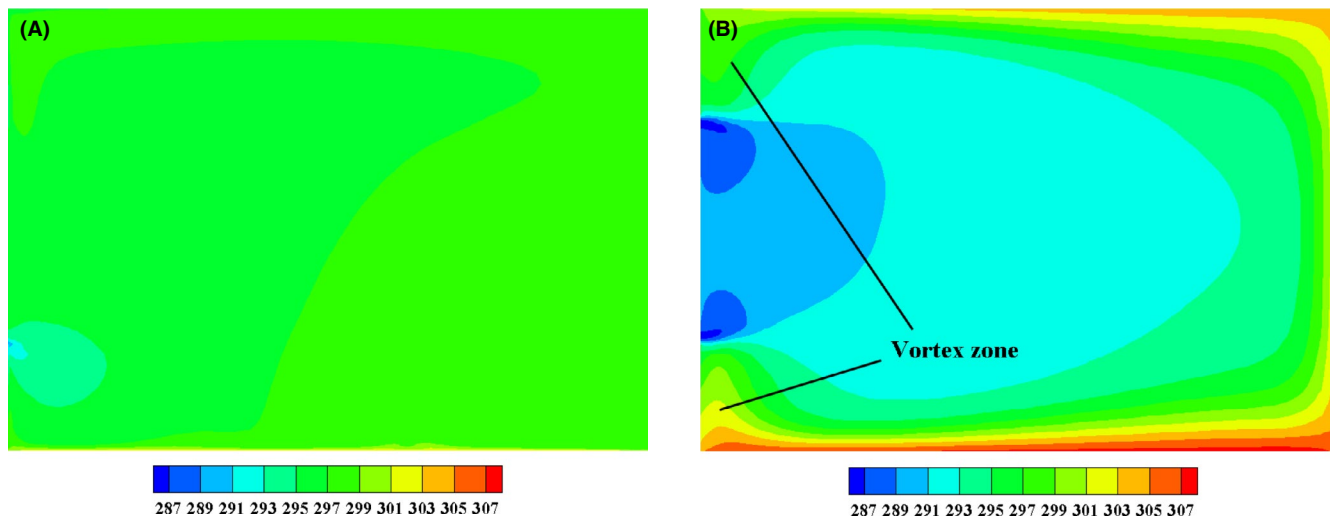
FIGURE 9 Temperature (K) contours on middle *z-x* cross-section at *y* = 1.8 m of the room after 1 day

gas-phase DEHP concentration near the floor in "off" case is higher than that in "on" case. Moreover, temperature also shows an impact on several physical properties, such as mass transfer coefficient in Equation (13), Brownian diffusion coefficient in Equation (25), and DEHP diffusion coefficient in Equation (10).

From Figures 6 and 7, it is obvious that increase of indoor particle concentration, enhancement of heat transfer, weaken of mass transfer and the air infiltration through window gap all contribute to decrease gas-phase DEHP concentration. The increase of the indoor particle concentration will result in an enhancement of transfer rate from gas-phase to particle-phase DEHP which will be purified by air cleaner or deposition onto the wall. The enhancement of heat transfer will reduce the temperature and the gas-phase DEHP concentration near the emission surface (or steady DEHP concentration). The weakening of convection will reduce the mass transfer rate of DEHP to the absorption wall. The fresh air infiltrated through window gap will slow the emission of DEHP to higher positions in the room. Statistical results from Figures 6 and 7 show that average gas-phase DEHP concentrations of "on" case and "off" case during the 20th~70th days are 0.389 and 0.232 $\mu g/m^3$, respectively. This is because, gas-phase DEHP concentration near the emission surface is lower in "on" case (in average, 4.752 $\mu g/m^3$ in "off" case and 2.473 $\mu g/m^3$ in "on" case during the 20th~70th days, which contribute to a lower steady DEHP concentration) while the convection effect is more obvious (which contribute to a higher DEHP transport rate) compared with these in "off" case. Moreover, average particle-phase DEHP concentrations of "on" case and "off" case during the 20th ~70th days are 6.58 × 10^{-3} and 0.282 $\mu g/m^3$ respectively. The extremely low particle-phase DEHP concentration in "on" case is due to the air cleaner purification effect for particle-phase DEHP.

Figures 10A and B give the PM2.5 concentration distributions on the *z-x* cross-section at *y* = 0.14 m of the room and room middle *x-z* cross-section at *y* = 1.8 m after 1 day in "on" case. From Figures 6C and 7C, we can statistics that the average particle concentrations during the period from 20th to 70th days in "off" case and "on" case

are 47.21 and 3.379 $\mu g/m^3$, respectively. In "on" case, as shown in Figure 10, forced convection of air cleaner is dominant. The whole room is filled with the clean gas discharged from air cleaner, leading to fine PM2.5 purification. In addition, due to the existence of vortex, inertial separation effect of particle at the wall corner will promote the deposition of PM2.5 on the wall. In "off" case, as shown in Figure 11, gravity deposition process of suspended particles and vortexes caused by the infiltration wind are the main driving force of PM2.5 motion.

Figures 12 and 13 give gas-phase DEHP concentration distribution variations on the room middle *x-z* cross-section at *y* = 1.8 m in "on" case and "off" case, respectively. As shown in the figures, for "on" case room gas-phase DEHP concentration is nearly uniform and gradually increase (also see Figure 6A). In "off" case, at the initial time, gas-phase DEHP concentration near the floor increase rapidly due to the rise of temperature. Later, weak convection and turbulent diffusion cause an extremely slow emission process. At the corner near the window, gas-phase DEHP increase relatively faster due to the airflow vortexes. Clean air infiltrated through window gap restrain DEHP emitting into the whole room. Furthermore, high temperatures in the floor and walls cause high surface partition coefficients, leading to an enhanced emission surface concentration and absorption process.

Distributions of particle-phase DEHP concentration are given in Figure 14. From Figures 6 and 7, we can statistics that average relative particle-phase DEHP concentrations compared with the room average total DEHP concentration during day 20–70 in "off" case and "on" case are 0.282/(0.232 + 0.282) = 54.9% and 6.58 × 10^{-3}/(0.389 + 6.58 × 10^{-3}) = 1.7%, respectively. In "on" case, the low particle-phase DEHP concentration is simply because of the air cleaner purification effect of the carrier, suspended particle. In "off" case, due to the low fluid velocity, longer time is provided for the non-equilibrium absorption process into PM2.5, considering gravity settling, leading to a higher particle-phase DEHP concentration. Moreover, due to the effect of vortex, particle-phase DEHP
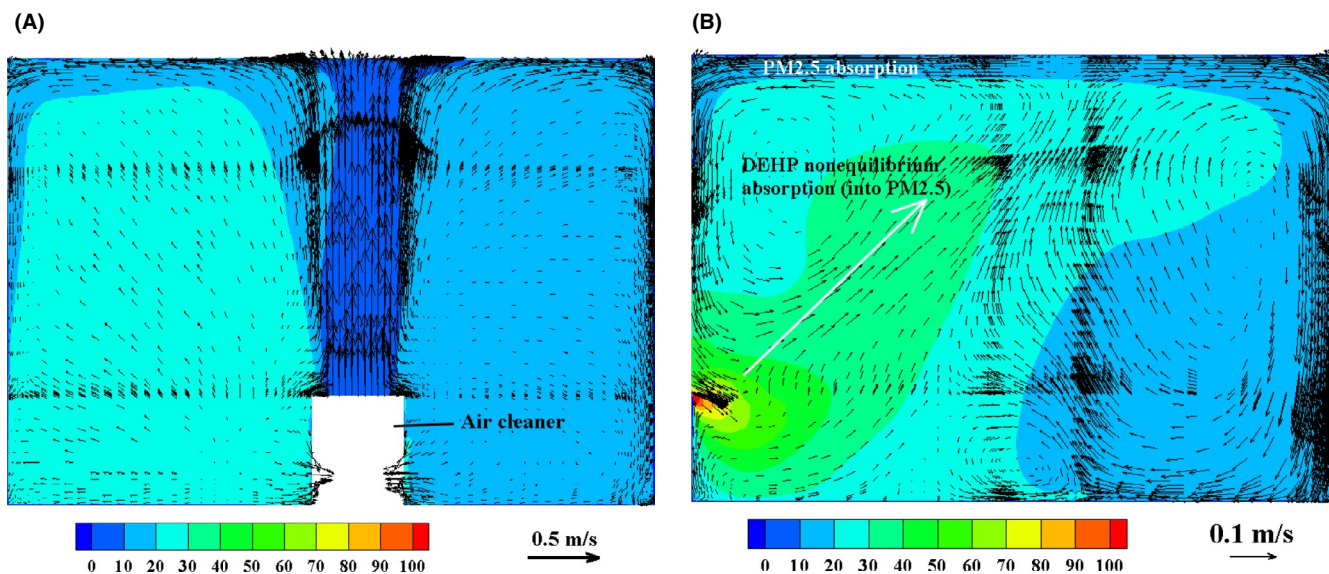
(A)

(B)

FIGURE 10   PM2.5 concentration (μg/m³) contours and velocity vector diagram after 1 day in air cleaner "on" case
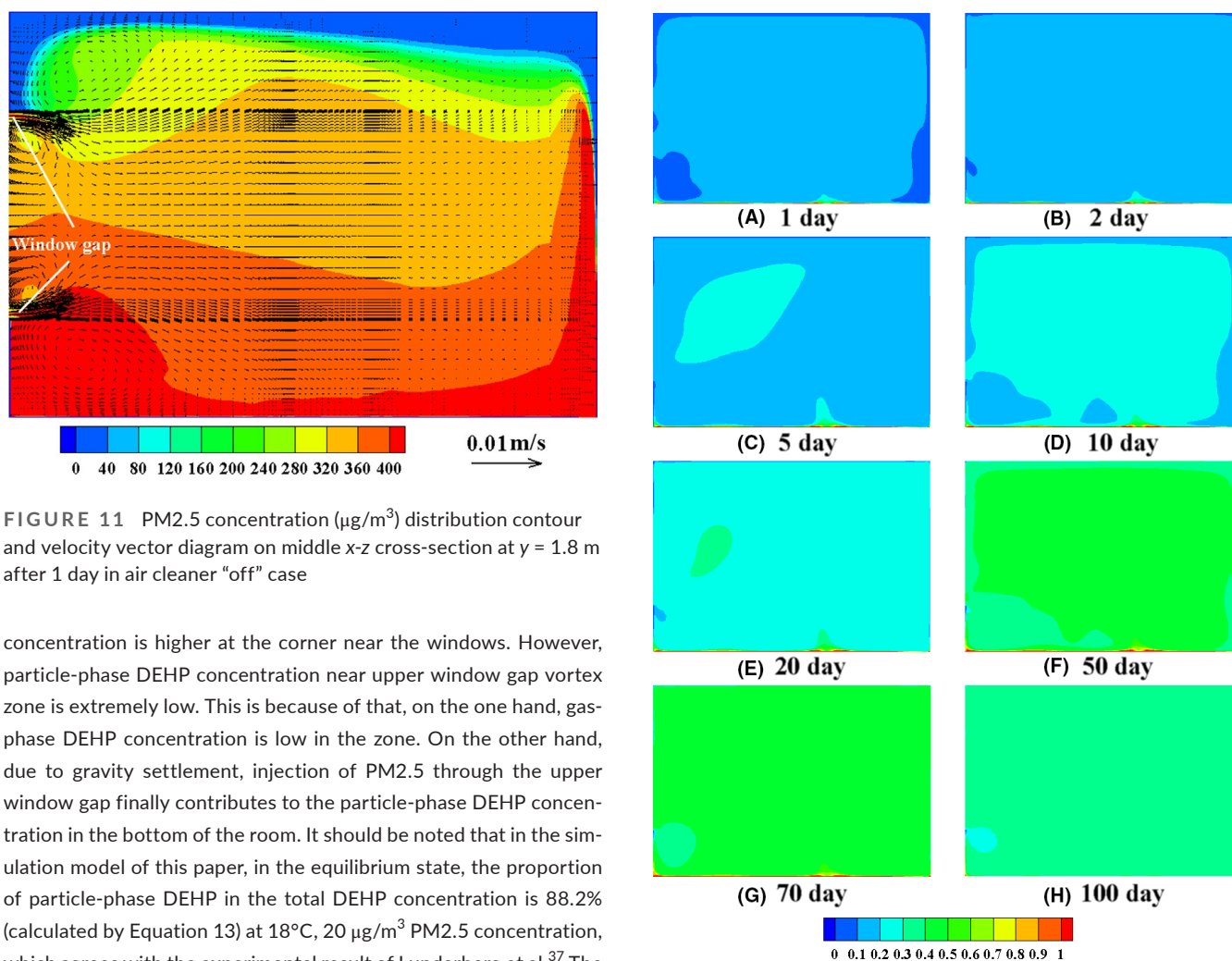

FIGURE 11   PM2.5 concentration (μg/m³) distribution contour and velocity vector diagram on middle *x-z* cross-section at *y* = 1.8 m after 1 day in air cleaner "off" case

concentration is higher at the corner near the windows. However, particle-phase DEHP concentration near upper window gap vortex zone is extremely low. This is because of that, on the one hand, gas-phase DEHP concentration is low in the zone. On the other hand, due to gravity settlement, injection of PM2.5 through the upper window gap finally contributes to the particle-phase DEHP concentration in the bottom of the room. It should be noted that in the simulation model of this paper, in the equilibrium state, the proportion of particle-phase DEHP in the total DEHP concentration is 88.2% (calculated by Equation 13) at 18°C, 20 μg/m³ PM2.5 concentration, which agrees with the experimental result of Lunderberg et al.[37] The simulated particle-phase DEHP proportion (53.6%) in this paper is lower than their experimental findings. The reasons are as follows. (1) Average temperature in our simulation is about 23.3°C, which is
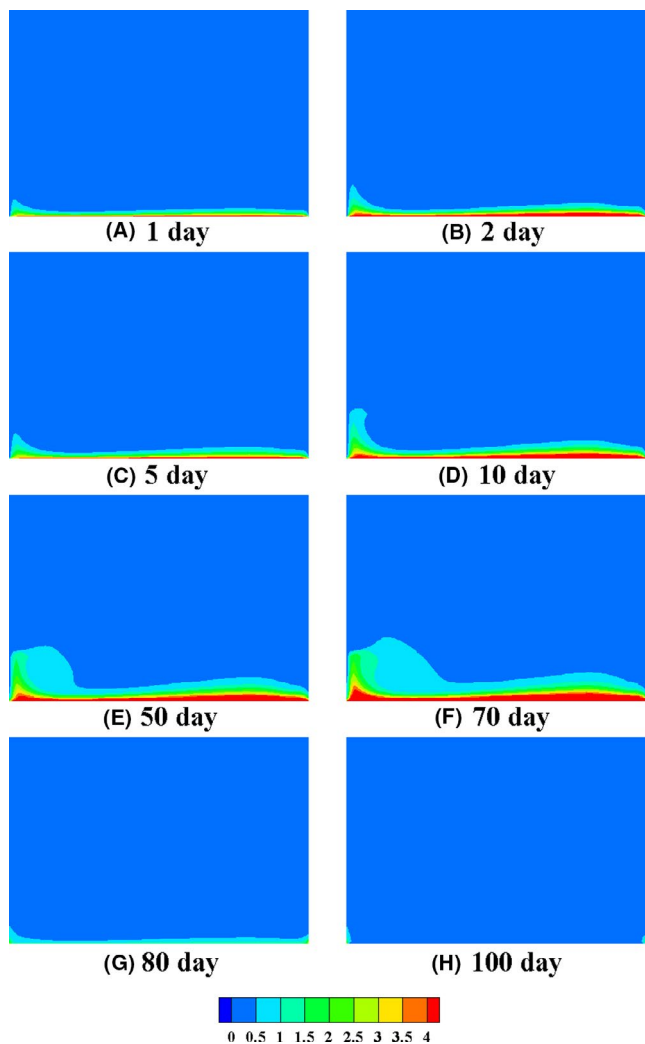

FIGURE 12   Gas-phase di-2-ethylhexyl phthalate (DEHP) concentration (μg/m³) distribution variation on middle *x-z* cross-section at *y* = 1.8 m in air cleaner "on" case

higher than that in Lunderberg's experiment. Equilibrium particle-phase DEHP proportion is only 72.2% at 23.3°C, 20 µg/m³ PM2.5 concentration. (2) The simulated particle-phase DEHP proportion (53.6%) is lower than the equilibrium value (72.2%). This is because in Lunderberg's experiment, during the vacant period, average DEHP concentrations are roughly equivalent between the indoors and outdoors.[37] Suspended particles are put in DEHP equilibrium-state concentration, leading to an adequate time for DEHP absorption process into particles. While in this simulation, the emission process from PVC floor is studied. In "off" case, gas-phase DEHP concentration near the emission surface is much higher than that in other regions, as is shown in Figure 7. When suspended particles move into the high concentration region, due to settlement and floor absorption, particles will be deposited onto the floor soon. DEHP absorption process from gas-phase to particle-phase is mainly performed in the low gas-phase DEHP concentration region. Partitioning speed of DEHP between the particles and gas is slow in the high gas-phase DEHP concentration region, causing that the DEHP absorption process into suspended particles doesn't reach the equilibrium state. These are the reasons why our simulated particle-phase DEHP proportion is lower than that in Lunderberg's experiment.

Finally, a comparison of non-isothermal model and isothermal model is developed. According to the simulation result of "off" case, average temperature of the whole room during 20th to 70th days is 23.3°C (isothermal model). Average temperatures of the floor, ceiling, and intermediate region (between surface $z = 0.5$ and surface $z = 1.55$) are 34.09, 29.87, and 22.09°C, respectively (non-isothermal model). Due to the complexity of the room-scale model, it is difficult to compare isothermal and non-isothermal model quantitatively in that scale. The above temperature is applied in FLEC model (Figure 4A) for comparison. Simulation results are shown in Figure 15. We can see that for the test FLEC, isothermal model will underestimate steady concentration by 82% and underestimate steady time
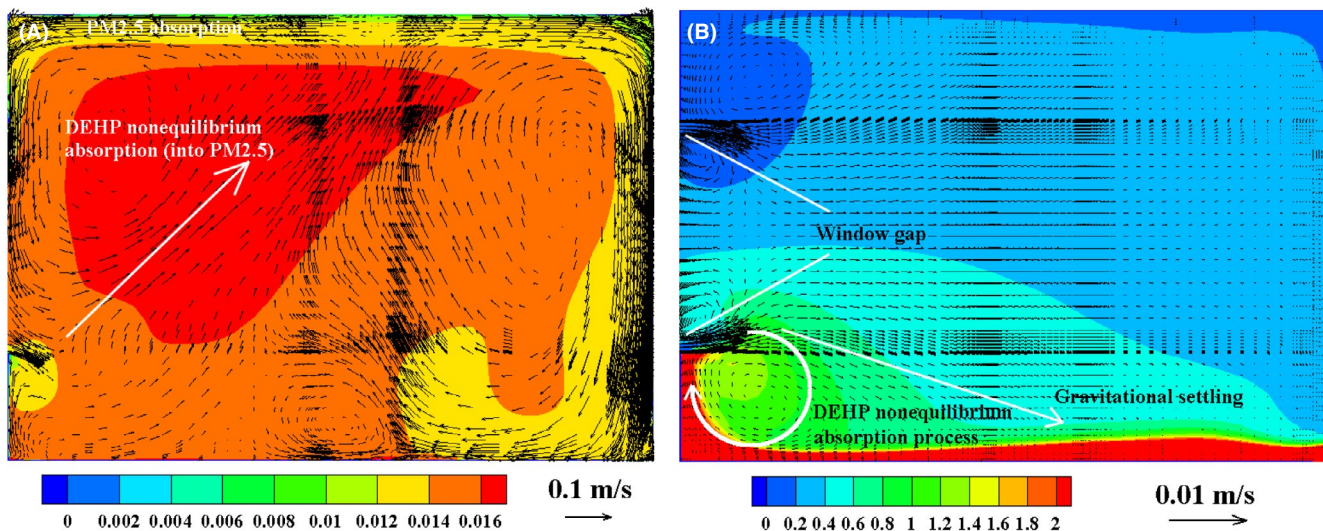

FIGURE 13 Gas-phase di-2-ethylhexyl phthalate (DEHP) concentration (µg/m³) distribution variation on middle x-z cross-section at y = 1.8 m in air cleaner "off" case

FIGURE 14 Particle-phase di-2-ethylhexyl phthalate (DEHP) concentration (µg/m³) distribution contour and velocity vector diagram on middle x-z cross-section at y = 1.8 m after 1 day
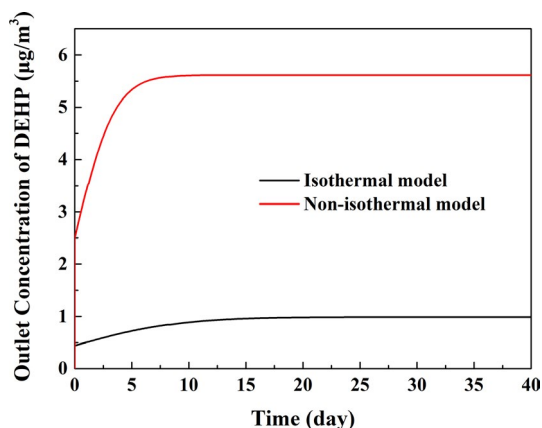
FIGURE 15 Comparison of isothermal and non-isothermal models

by 54% compared with the non-isothermal model, showing the necessity of the non-isothermal model in this circumstance.

4 | CONCLUSION

In this research, a 3-dimensional non-isothermal computational fluid dynamics model has been developed to study the emission process of DEHP in a room. The model considers turbulent flow field, absorption boundary of mass, convective and radiative heat transfer, particle motion, gas-phase, and particle-phase DEHP distribution. The SVOC transport processes in a 15 m^2 room in Beijing, including window gap, door gap, and floor heating, in 100 days when air cleaner "on" and "off" are simulated by the developed model. The predicted gas-phase and particle-phase DEHP distribution characteristics are analyzed. The main contributions and conclusions of this paper may be summarized in two aspects as follows:

1. From aspect of numerical prediction model, the major contributions of the present indoor SVOC transport numerical simulation are as follows:

1. Non-isothermal SVOC emission process prediction model is developed, including heat conduction, convection (natural convection and forced convection), and radiation heat transfer modes.
2. An irreversible first-order model is provided as absorption boundary condition of particle and particle-phase SVOCs in a real room and the necessity of this model is analyzed.
3. An inertia slip velocity is introduced into the particle and particle-phase SVOC motion governing equation.

2. From aspect of practical application:

1. Floor heating will promote the emission process at a wide range while wind infiltration through the window gap will restrain the overall emission process.
2. When air cleaner is always open, the final gas-phase DEHP concentration in the room tends to be uniform while the

emission process is far from equilibrium even emission process lasts 100 days when air cleaner is closed.

3. Increase of indoor particle concentration, enhancement of heat transfer, weaken of mass transfer, and the air infiltration through window gap all contribute to decrease gas-phase DEHP concentration.

CONFLICT OF INTEREST

The authors declare that they have no known competing financial interests or personal relationships that could have appeared to influence the work reported in this paper.

AUTHOR CONTRIBUTIONS

Wen-Quan Tao: Conceptualization (equal); Funding Acquisition (lead); Project Administration (equal); Resources (lead); Supervision (equal); Writing – Original Draft Preparation (supporting); Writing – Review & Editing (lead). Fan Bai: Conceptualization (equal); Data Curation (lead); Formal Analysis (lead); Investigation (lead); Methodology (lead); Software (lead); Validation (lead); Visualization (lead); Writing – Original Draft Preparation (lead); Writing – Review & Editing (equal). Hao Ding: Methodology (supporting); Writing – Original Draft Preparation (equal). Yu-Tong Mu: Project Administration (equal); Supervision (equal). Yan-Jun Dai: Methodology (supporting). Yin-Ping Zhang: Project Administration (supporting); Methodology (supporting).

PEER REVIEW

The peer review history for this article is available at https://publons.com/publon/10.1111/ina.12849.

ORCID

Fan Bai https://orcid.org/0000-0002-2291-2495
Wen-Quan Tao https://orcid.org/0000-0002-2348-6299

REFERENCES

1. World Health Organization (WHO). Indoor air quality: Organic pollutants. EURO Reports and Studies No III, World Health Organization, Copenhagen, Denmark; 1989.
2. Tilson HA, Veronesi B, McLamb RL, Matthews HB. Acute exposure to tris (2-chloroethyl) phosphate produces hippocampal neuronal loss and impairs learning in rats. *Toxicol Appl Pharmacol.* 1990;106(2):254-269.
3. Latini G. Monitoring phthalate exposure in humans. *Clin Chim Acta.* 2005;361(1-2):20-29.

4. Clausen PA, Hansen V, Gunnarsen L, Afshari A, Wolkoff P. Emission of di-2-ethylhexyl phthalate from PVC flooring into air and uptake in dust: emission and sorption experiments in FLEC and CLIMPAQ. *Environ Sci Technol*. 2004;38(9):2531-2537.

5. Clausen PA, Liu Z, Kofoed-Sørensen V, Little J, Wolkoff P. Influence of temperature on the emission of di-(2-ethylhexyl) phthalate (DEHP) from PVC flooring in the emission cell FLEC. *Environ Sci Technol*. 2012;46(2):909-915.

6. Clausen PA, Xu Y, Kofoed-Sørensen V, Little JC, Wolkoff P. The influence of humidity on the emission of di-(2-ethylhexyl) phthalate (DEHP) from vinyl flooring in the emission cell "FLEC". *Atmos Environ*. 2007;41(15):3217-3224.

7. Ekelund M, Azhdar B, Gedde UW. Evaporative loss kinetics of di (2-ethylhexyl) phthalate (DEHP) from pristine DEHP and plasticized PVC. *Polym Degrad Stab*. 2010;95(9):1789-1793.

8. Schnelle-Kreis J, Sklorz M, Orasche J, Stölzel M, Peters A, Zimmermann R. Semi volatile organic compounds in ambient PM2.5. Seasonal trends and daily resolved source contributions. *Environ Sci Technol*. 2007;41(11):3821-3828.

9. Liang Y, Caillot O, Zhang J, Zhu J, Xu Y. Large-scale chamber investigation and simulation of phthalate emissions from vinyl flooring. *Build Environ*. 2015;89:141-149.

10. Xu Y, Little JC. Predicting emissions of SVOCs from polymeric materials and their interaction with airborne particles. *Environ Sci Technol*. 2006;40(2):456-461.

11. Hu K, Chen Q, Hao JH. Influence of suspended particles on indoor semi-volatile organic compounds emission. *Atmos Environ*. 2013;79:695-704.

12. Chen Q, Hu K. Prediction model for SVOCs transport in the air and interactions with airborne particles. *Atmos Environ*. 2014;96:61-69.

13. Hu K, Chen Q. Ventilation optimization for reduction of indoor semi-volatile organic compound concentration based on the variational principle. *Build Environ*. 2015;94:676-682.

14. Mao YF, Li Z, He YL, Tao WQ. CFD analysis of SVOC mass transfer in different chambers. *Int J Heat Mass Transfer*. 2016;99:613-621.

15. Liu C, Shi S, Weschler C, Zhao B, Zhang Y. Analysis of the dynamic interaction between SVOCs and airborne particles. *Aerosol Sci Technol*. 2013;47(2):125-136.

16. Wolkoff P, Clausen PA, Nielsen PA, Gunnarsen L. Documentation of field and laboratory emission cell "FLEC": identification of emission processes from carpet, linoleum, paint, and sealant by modeling. *Indoor Air*. 1993;3(4):291-297.

17. Mao YF, Li Z, Zhang YP, He YL, Tao WQ. A review of mass-transfer models and mechanistic studies of semi-volatile organic compounds in indoor environments. *Indoor Built Environ*. 2018;27(10):1307-1321.

18. Wu X, Olesen BW, Fang L, Zhao J. A nodal model to predict vertical temperature distribution in a room with floor heating and displacement ventilation. *Build Environ*. 2013;59:626-634.

19. Wang YF, Huai WX. Random walk particle tracking simulation on scalar diffusion with irreversible first-order absorption boundaries. *Environ Sci Pollut Res*. 2019;26(32):33621-33630.

20. Wang M. Modeling airflow and contaminant transport in enclosed spaces with advanced models (Doctoral dissertation, Purdue University).

21. Chen C, Liu W, Li F, et al. A hybrid model for investigating transient particle transport in enclosed environments. *Build Environ*. 2013;62:45-54.

22. Tao WQ. *Numerical Heat Transfer*. Xi'an: Xi'an Jiaotong University Press; 2001 (in Chinese).

23. Zhao B, Yang C, Yang X, Liu S. Particle dispersion and deposition in ventilated rooms: testing and evaluation of different Eulerian and Lagrangian models. *Build Environ*. 2008;43(4):388-397.

24. Gray DD, Giorgini A. The validity of the Boussinesq approximation for liquids and gases. *Int J Heat Mass Transfer*. 1976;19(5):545-551.

25. Chmielewski M, Gieras M. Three-zonal wall function for k-ε turbulence models. *Comput Methods Sci Technol*. 2013;19(2):107-114.

26. Shih TH, Liou WW, Shabbir A, Yang Z, Zhu J. A new k-ε eddy viscosity model for high Reynolds number turbulent flows. *Comput Fluids*. 1995;24(3):227-238.

27. Kays WM. Convective heat and mass transfer. Tata McGraw-Hill Education; 2011:260-261.

28. Fluent help file; 2020. https://ansyshelp.ansys.com

29. Gao NP, Niu JL. Modeling particle dispersion and deposition in indoor environments. *Atmos Environ*. 2007;41(18):3862-3876.

30. Lyman WJ, Reehl WF, Rosenblatt DH (publisher). *Handbook of Chemical Property Estimation Methods: Environmental Behavior of Organic Compounds*. New York, NY: McGraw-Hill; 1982 (Chapter 17).

31. Cao J, Eichler CMA, Wu Y, Little JC. Dynamic method to measure partition coefficient and mass accommodation coefficient for gas-particle interaction of phthalates. *Aerosol Sci Technol*. 2019;53(10):1158-1171.

32. Zhang Y, Luo X, Wang X, Qian K, Zhao R. Influence of temperature on formaldehyde emission parameters of dry building materials. *Atmos Environ*. 2007;41(15):3203-3216.

33. Manoukian A, Buiron D, Temime-Roussel B, Wortham H, Quivet E. Measurements of VOC/SVOC emission factors from burning incenses in an environmental test chamber: influence of temperature, relative humidity, and air exchange rate. *Environ Sci Pollut Res*. 2016;23(7):6300-6311.

34. Elghobashi S. On predicting particle-laden turbulent flows. *Appl Sci Res*. 1994;52(4):309-329.

35. Alletto M, Breuer M. One-way, two-way and four-way coupled LES predictions of a particle-laden turbulent flow at high mass loading downstream of a confined bluff body. *Int J Multiphase Flow*. 2012;45:70-90.

36. Hinds WC. *Aerosol Technology: Properties, Behavior, and Measurement of Airborne Particles*. New York, NY: John Wiley & Sons; 1999.

37. Lunderberg DM, Kristensen K, Liu Y, et al. Characterizing airborne phthalate concentrations and dynamics in a normally occupied residence. *Environ Sci Technol*. 2019;53(13):7337-7346.

38. Zhao B, Wu J. Modeling particle deposition from fully developed turbulent flow in ventilation duct. *Atmos Environ*. 2006;40(3):457-466.

39. Thatcher TL, Lai AC, Moreno-Jackson R, Sextro RG, Nazaroff WW. Effects of room furnishings and air speed on particle deposition rates indoors. *Atmos Environ*. 2002;36(11):1811-1819.

40. Meng CP. Polycyclic aromatic hydrocarbons pollution compositions of fine particles (PM2.5) and particle size distribution in indoor environment. (Master dissertation, Shandong University, 2013, Chapter 4, in Chinese).

41. Howell JR, Menguc MP, Siegel R. *Thermal Radiation Heat Transfer*, 6th ed. Boca Raton, FL: CRC Press; 2015 (Chapters 4 and 5).

42. Hu J. Numerical simulation of building's heating and indoor condition under the condition of natural weather. (Master dissertation, Tianjin University, 2005, Chapters 3 and 5, in Chinese).

43. Zhang LZ, Niu JL. Laminar fluid flow and mass transfer in a standard field and laboratory emission cell. *Int J Heat Mass Transfer*. 2003;46(1):91-100.

44. Xu Y, Liu Z, Park J, Clausen PA, Benning JL, Little JC. Measuring and predicting the emission rate of phthalate plasticizer from vinyl flooring in a specially-designed chamber. *Environ Sci Technol*. 2012;46(22):12534-12541.

SUPPORTING INFORMATION

Additional supporting information may be found online in the Supporting Information section.